



Strong Spatial Aggregation of Martian Surface Temperature Shaped by Spatial and Seasonal Variations in Meteorological and Environmental Factors

Yao-Wen Luo¹, Fei Li^{1,2,*}, Jian-Guo Yan^{2,*} , and Jean-Pierre Barriot^{2,3}

¹ Chinese Antarctic Center of Surveying and Mapping, Wuhan University, Wuhan, 430070, China; yaowenluo@whu.edu.cn

² State Key Laboratory of Information Engineering in Surveying, Mapping and Remote Sensing, Wuhan University, Wuhan, 430070, China; fli@whu.edu.cn, jgyan@whu.edu.cn

³ Observatoire Geodesique de Tahiti, University of French Polynesia, BP 6570, F-98702 Faa'a, Tahiti, French Polynesia; jean-pierre.barriot@upf.pf

Received 2021 August 11; revised 2021 October 2; accepted 2021 October 9; published 2022 January 21

Abstract

Spatio-temporal variation in the Martian surface temperature (MST) is an indicator of ground level thermal processes and hence a building block for climate models. However, the distribution of MST exhibits different levels of spatial aggregation or heterogeneity, and varies in space and time. Furthermore, the effect of regional differences in meteorological or environmental factors on the MST is not well understood. Thus, we investigated the degree of spatial autocorrelation of MST across the surface of Mars globally by Moran's I, and identified the hot spots by GetisOrd G_i^* . We also estimated the regional differences in the influence of seasonally dominant factors including thermal inertia (TI), albedo, surface pressure, latitude, dust and slope on MST by a geographically weighted regression model. The results indicate (1) that MST is spatially aggregated and hot and cold spots varied over time and space. (2) Hemispheric differences in topography, surface TI and albedo were primarily responsible for the hemispheric asymmetry of hot spots. (3) The dominant factors varied by geographical locations and seasons. For example, the seasonal Hadley circulation dominates at the low-latitudes and CO₂ circulation at the high-latitudes. (4) Regions with extreme variations in topography and low TI were sensitive to meteorological and environmental factors such as dust and CO₂ ice. We conclude that the spatial autocorrelation of MST and the spatial and seasonal heterogeneity of influencing factors must be considered when simulating Martian climate models. This work provides a reference for further exploration of Martian climatic processes.

Key words: methods: analytical – planets and satellites: surfaces – methods: statistical – planets and satellites: fundamental parameters

1. Introduction

Martian surface temperature (MST) is an indicator of the energy budget of the planetary surface. Moreover, the potential existence of life and liquid water might be strongly related to temperature on the Martian surface (Kieffer et al. 1977). Analysis of the surface temperature of Mars could aid exploration and help answer the question if Mars has or had the ambient conditions to support life. In addition, surface temperature variation is directly related to thermophysical properties of the shallow subsurface (Hamilton et al. 2014). As such, surface temperature analysis could provide insight into the physical properties and processes of Martian subsurface material that might not be observable on the ground. Moreover, an understanding of the spatial and temporal variation in the MST adds insights into the thermal behavior of near-surface elements from the local to regional scale, as well as shedding light on the geological and land surface physical processes occurring on Mars (Read et al. 2015; Spanovich et al. 2006; Tosi et al. 2019).

The distribution of MST is not stable over time and space. Observations into the surface temperature on Mars revealed huge seasonal variations (Leovy 2001; Spanovich et al. 2006) and regional asymmetries in the surface temperature (Kieffer et al. 1972, 1976; Miller et al. 2018; Kass et al. 2020). MST and ground surface thermal properties vary from one region to another (Martínez et al. 2017; Mellon et al. 2000; Spanovich et al. 2006; Putzig & Mellon 2007). Measurements by the Viking lander and Curiosity rover at Gale Crater show a large difference in the average daily temperature during a Martian year (Siegler et al. 2017). These asymmetries of MST over seasons and locations are generally attributed to solar radiation determined by the Martian orbital eccentricity (Read et al. 2015; Zurek et al. 1992). In general, the spatial distribution of geographical elements is not independent, but exhibits a certain degree of spatial dependence, that is, the near observations are more related than distant observations (Tobler 1970); however, the investigation to date regarding the spatial autocorrelation patterns of MST has received little attention.

The surface temperature on Mars is not randomly distributed in space, but shows patterns of spatial aggregation. The spatial autocorrelation can measure the correlation among observations

* Corresponding authors.

based on the distance they are apart (Getis 2010). Quantitative measurement of spatial autocorrelation can be used to diagnose whether the distribution of surface temperature is concentrated, dispersed or random, as well as the degree of spatial aggregation of surface temperature. Ignoring the spatial autocorrelation of surface temperature could reduce the accuracy of the Martian near-surface climate models. Quantitative measurements of spatial autocorrelation of surface temperature at both global and local scales could provide valuable reference for both theoretical and applied studies of the Martian near surface environment as it is yet not clear which climatological and/or geographical factors could explain the spatial autocorrelation of the surface temperature.

Understanding the meteorological or environmental factors controlling or influencing the variation in MST is a focus in Martian climate studies. Previous research have shown that environmental factors, including topography (Miller et al. 2018; Millot et al. 2021), dust (Gurwell et al. 2005; Kass et al. 2016, 2020), atmospheric circulation (Leovy 2001; Richardson & Wilson 2002; Spiga & Forget 2009; Zalucha et al. 2010), surface albedo (Fenton et al. 2007), thermal inertia (TI, Jakosky et al. 2000; Petrosyan et al. 2011; Piqueux & Christensen 2011; Putzig & Mellon 2007; Savijarvi 1999; Vasavada et al. 2017), CO₂ (Hunt 1980; Pierrehumbert 2010), etc., influence the MST distribution pattern. However, most of the previous studies have focused on the relations between a single factor and MST, and they have rarely quantitatively analyzed the relationships between multiple factors and surface temperature at a large scale. In addition, the spatial and seasonal variations of the possible factors and processes that could account for the surface temperature spatial autocorrelation have also been largely overlooked. Much less emphasis has been directed toward the spatio-temporal variation of the relationships between surface temperature and affecting factors. The surface temperature and related affecting factors manifest great spatial heterogeneity and seasonal changes in the real world. Thus, the relationship between the MST and its influencing factors is not stable over space but varies by geographical locations and seasons.

To fill these gaps, we relied on geographic information system (GIS) in conjunction with statistical methods to address the patterns of spatial autocorrelation in the MST and its relationships with the potential to influence near surface environmental factors, and variations over locations and seasons. The aim of this study is fourfold: (1) to investigate the degree of spatial autocorrelation of the Global monthly MST during Martian years 30–32; (2) to map surface temperature's hot spots (clusters of high data values) and cold spots (clusters of low data values) locally over the global Martian surface and their variation over space and time; (3) to quantitatively determine the effect of each potential driving factor on surface temperature seasonally from a global and local perspective respectively; (4) to map the coefficients of

each possible factor that accounts for spatial pattern and seasonal changes of MST and to demonstrate that the relationships between MST and its affecting factors are heterogeneous over space and seasons. Evaluation of the spatial autocorrelation of MST and the spatio-temporal heterogeneity of the influence of driving factors on it is a first step toward improving Martian near-surface climate simulation models, as well as contributing to deepening our knowledge of the near-surface environmental characteristics of Mars.

2. Data and Method

2.1. Study Area and Data Source

This study took the global surface temperature of Mars as the research object. The spatial pattern of MST exhibits spatial heterogeneity as depicted in Figure 1.

As illustrated in Figure 1, Mars was divided into $5^\circ \times 5^\circ$ grids to ensure that the main components were recorded. In total, 2592 grids were generated as the basic spatial units. Considering the availability of data and their continuity in time, the study period was Martian years 30–32, corresponding to the Earth period 2009 October 27 to 2015 June 18. The description of the data we used in this study is presented in Table 1.

As described in Table 1, the gridded climate data set including ST (surface temperature), Ps (surface pressure), CO₂ (surface CO₂ ice) and dust during Martian years 30–32 were collected from the Open access to Mars Assimilated Remote Soundings (OpenMARS) database (Holmes et al. 2020). This product provides climate data every 2 Martian hours with a spatial resolution of $5^\circ \times 5^\circ$. The HRSC and MOLA Blended Digital Elevation Model (DEM) at 200 m resolution was derived from the Astrogeology PDS Annex, U.S. Geological Survey (Ferguson et al. 2018). We extracted the Martian topographic elevation and slope data from the Blended Digital Elevation Model using arcgis10.7 tools. The nighttime surface TI map (Putzig & Mellon 2007) with a resolution of 20 pixel per degree was collected by Planetary Science Institute (<https://sharad.psi.edu/inertia/>). The surface albedo data (Christensen et al. 2001) with a resolution of 7400 m was taken from the Astrogeology Science Center data (https://astrogeology.usgs.gov/search/map/Mars/GlobalSurveyor/TES/Mars_MGS_TES_Albedo_mosaic_global_7410m).

This study used Excel, Python and R software for data preprocessing, and Geoda, R and ArcGIS10.7 software for analysis and mapping. All of the data considered in the present research were transformed into the Mars 2000 Coordinate System. Due to the different spatial resolutions, all the data were uniformly transformed to the same spatial size with horizontal $5^\circ \times 5^\circ$ grid scale using Zonal Statistics Tool in ArcGIS10.7. According to Table 2, three sorts of data sets including Martian months (in total 12 months), Martian seasons including spring, summer, fall and winter and the Martian year

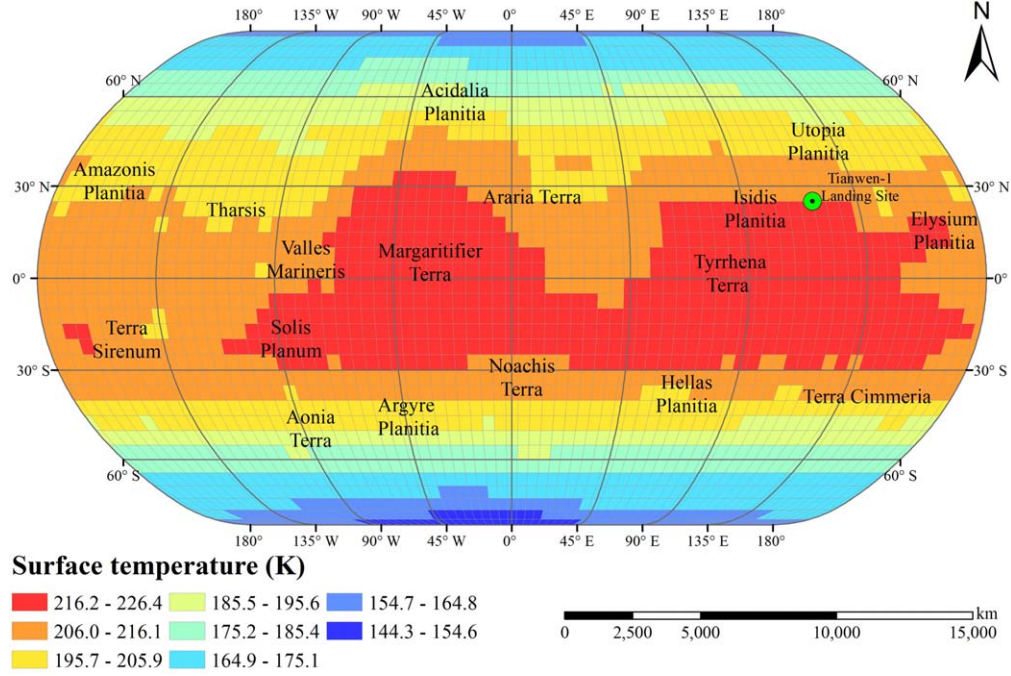


Figure 1. Distribution of Martian average surface temperature during Martian years 30–32.

30–32 statistical data sets were preprocessed and used for modeling and analysis.

2.2. Spatial Autocorrelation Analysis

2.2.1. Global Moran's I

The Moran's Index (Moran's I, Moran 1950) is one of the most popular methods to measure the degree of spatial autocorrelation. It quantifies the spatial aggregation between features by assessing the correlation of attributes between individual features and their surrounding neighbors. The expression for global Moran's I can be expressed as in Equation (1)

$$I = \frac{n \sum_{i=1}^n \sum_{j=1}^n w_{ij} (x_i - \bar{x})(x_j - \bar{x})}{\left(\sum_{i=1}^n \sum_{j=1}^n w_{ij} \right) \sum_{i=1}^n (x_i - \bar{x})^2} \quad (1)$$

where n equals the total number of spatial units in this study, x_i and x_j are the surface temperature of the spatial units at geographical locations i and j , respectively, \bar{x} is the mean value of the surface temperature in the whole study area, and w_{ij} is the the spatial weight between the spatial units at locations i and j . Generally, when spatial units i and j are adjacent, $w_{ij} = 1$; when they are are not adjacent, the weight w_{ij} is given the value of 0.

The significance of the global Moran's I is validated by z -score and p -value. The z -score is calculated with the following

equation

$$Z = \frac{I - E[I]}{\sqrt{V[I]}} \quad (2)$$

where

$$E[I] = -1/(n - 1) \quad (3)$$

$$V[I] = E[I^2] - E[I]^2 \quad (4)$$

In this study, the global Moran's I was utilized to evaluate the degree of spatial autocorrelation in the MST at the global scale for each Martian month during Martian years 30–32 based on 9999 permutations with the significance level $p < 0.001$. The value of Moran's I ranges from -1 to 1 . A positive Moran's I value indicates that the MST observations are clustered spatially. When the value approaches 1 , the clustering pattern is stronger. On the contrary, a negative Moran's I value signifies the MST exhibits a negative spatial correlation, and the pattern observed is scattered or spatially dispersed. When its value approaches -1 , the negative spatial correlation is strong. When the value of Moran's I equals 0 , the MST is randomly distributed in the study area.

2.2.2. Hot Spot Analysis: GetisOrd G_i^* Statistic

The global Moran's I quantifies the pattern of spatial autocorrelation over an entire study area, but cannot capture the pattern of spatial autocorrelation at the local scale. The GetisOrd G_i^* proposed by Ord & Getis (1995), also known as hot-spot analysis, is one means to quantify localized

Table 1
Description of the Data used in this Study

Variables	Data Description	Scale	Unit	Spatial Resolution	Data source
ST	Surface temperature	Hourly	K	5° × 5°	https://ordo.open.ac.uk/articles/data_set/OpenMARS_MY28-32_standard_database/7352579?backTo=/collections/OpenMARS_database/4278950
Ps	Surface pressure	Hourly	Pa	5° × 5°	
CO ₂	Surface CO ₂ ice	Hourly	kg m ⁻²	5° × 5°	
Dust	Visible column dust optical depth	Hourly	NU	5° × 5°	
TI	Nightside surface thermal inertia	Yearly	tiu	20 pixel per degree	https://sharad.psi.edu/inertia/
Albedo	Surface albedo	Yearly		7400 m	https://astrogeology.usgs.gov/search/map/Mars/GlobalSurveyor/TES/Mars_MGS_TES_Albedo_mosaic_global_7410m
Elevation	Topographic elevation data extracted from DEM of 200 m resolution	Yearly	meter	7400 m	https://astrogeology.usgs.gov/search/map/Mars/Topography/HRSC_MOLA_Blend/Mars_HRSC_MOLA_BlendDEM_Global_200mp_v2
Slope	Topographic slope data extracted from DEM (200 m resolution)	Yearly	Degree (°)	200 m	
Latitude	Martian latitude		Degree (°)		

4

Table 2
Calendar of Martian Seasons and Months

Season (Northern Hemisphere)	Season (Southern Hemisphere)	Month number	Solar longitude (Ls) range (degree)	
Spring	Autumn	1	0	30
		2	30	60
		3	60	90
Summer	Winter	4	90	120
		5	120	150
		6	150	180
Autumn	Spring	7	180	210
		8	210	240
		9	240	270
Winter	Summer	10	270	300
		11	300	330
		12	330	360

variation in the pattern of spatial autocorrelation. This method identifies hot spots (high–high value clusters) and cold spots (low–low value clusters) over the whole region by evaluating the degree of similarity between the attributes of each feature and that of its neighbors in this case, surface temperature. In this study, the GetisOrd G_i^* values were calculated for each $5^\circ \times 5^\circ$ grid cell and divided into hot spots and cold spots. Thus, a spatial unit with a high surface temperature may not be a statistically significant hot spot. In this study, a grid cell defined as a statistically significant hot spot should not only have a high surface temperature, but also must be surrounded by other grid cells with high surface temperature (with a similar definition for a cold spot). The GetisOrd G_i^* can be expressed as follows

$$G_i^* = \frac{\sum_{j=1}^n w_{ij} x_j - \bar{x} \sum_{j=1}^n w_{ij}}{s \sqrt{\frac{n \sum_{j=1}^n w_{ij}^2 - (\sum_{j=1}^n w_{ij})^2}{n-1}}} \dots \quad (5)$$

where x_j is the surface temperature of the spatial unit j , w_{ij} denotes the spatial weight between the spatial units i and j , and n is equal to the total number of spatial units in the study area, and

$$\bar{x} = \frac{\sum_{j=1}^n x_j}{n} \quad (6)$$

$$s = \sqrt{\frac{\sum_{j=1}^n x_j^2}{n} - \bar{x}^2} \quad (7)$$

In this study, GetisOrd G_i^* was utilized to identify hot and cold spots of the MST across the whole study area for each Martian month during Martian years 30–32. All the GetisOrd G_i^* indices were performed based on 9999 permutations. The degree of clustering and statistical significance of GetisOrd G_i^* was evaluated by z -score. A high positive z -score signifies spatial clusters among high surface temperature hot spots and a

small negative z -score indicates spatial clusters among low surface temperature cold spots.

2.3. Regression Models

2.3.1. Random Forests (RF)

To estimate the global relationship between MST and potential affecting factors, we used one of the most popular machine learning methods of random forests (RFs), proposed by Breiman (2001). The RF is a nonparametric model that captures non-linear relationships between variables more effectively than linear regression models (Smith et al. 2013). It is an improved ensemble machine learning algorithm comprised of many decision trees for regression and classification. Each decision tree in an RF is built by randomly selecting a set of variables and samples from the training data set. About 36.8% of the samples (spatial units) are not used, which are called the out-of-bag (OOB) data. In the RF regression, the mean square error (MSE) reduction method is the most applied method to estimate the variable importance (Ishwaran 2007; Strobl et al. 2007, 2008; Grömping 2009). The MSE reduction method estimates the variable importance considering the MSE value from the OOB data (Strobl et al. 2008; Cai et al. 2018). The steps for calculating variable importance of potential affecting variables of MST is determined as follows:

(1) Calculate the MSE of the OOB data for each decision tree. The MSE for OOB data of the decision tree can be calculated by Equation (8)

$$MSE_t = \frac{1}{N_t} \sum_{i=1}^{N_t} (y_i - \hat{y}_{i,t})^2 \quad (8)$$

where N_t is the number of spatial units of the OOB data in the tree t and $y_{i,t}$ is the prediction of the MST of the i th spatial unit for tree t .

(2) The target variable k is randomly replaced, and then the corresponding value of the MSE for the new tree t is calculated by Equation (9)

$$MSE_t(k) = \frac{1}{N_t} \sum_{i=1}^{N_t} (y_i - \hat{y}_{i,t}(k))^2 \quad (9)$$

where $\hat{y}_{i,t}(k)$ is the prediction of the MST for the i th spatial unit of the new tree t with the target variable k randomly replaced.

(3) Calculate the MSE reduction between MSE_t and $MSE_t(k)$. The variable importance for variable k of the decision tree t can be obtained from the MSE reduction results. The variable importance (VI) of variable k is the average MSE reduction of all trees in the RF, and expressed as Equation (10)

$$VI(k) = MSE(k) = \frac{1}{n} \sum_{t=1}^n (MSE_t - MSE_t(k)) \quad (10)$$

where n is equal to the total number of decision trees of an RF. We implemented the RF in the ‘‘RandomForest’’ package

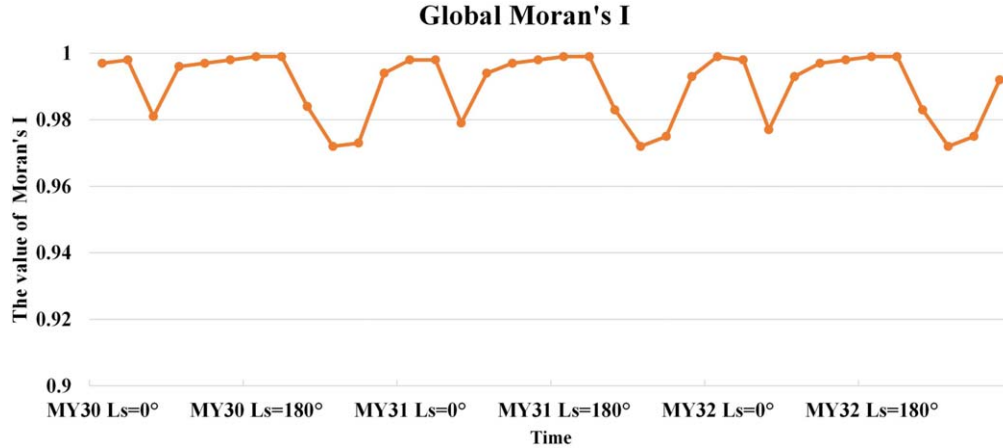


Figure 2. The trend of global spatial autocorrelation for MST during Martian years 30–32.

(Liaw & Wiener 2002) within R software (R Development Core Team, 2009). Seventy percent of the data was used for testing and 30 percent for training. Two parameters need to be optimized in an RF: *ntree*, the number of decision trees; and *mtry*, the number of candidate split variables at each node. To find the optimum *ntree* and *mtry* values for the RF modeling, *ntree* values were tested from 500 to 2000 with an interval of 100, while the *mtry* was tested from 1 to 7 with an interval of 1.

2.3.2. Geographically Weighted Regression Model

Global multivariate regression models such as RF and ordinary least squares (OLS) models have been widely applied in modeling and estimating the relationships among a couple of variables. These global models assume that the variables are spatially homogeneous, so they just evaluate a set of consistent regression parameters for all data. However, spatial features and their attributes are usually heterogeneous over space; global models may hide potentially important local variations in the relationships between variables. The geographically weighted regression (GWR) model (Brunsdon et al. 1996; Fotheringham et al. 2003) is an extension of OLS that addresses the spatial non-stationarity of variables, and could expose specific relationships among variables for every local region. Thus, the GWR model captures the variation of parameters with geographical location by adding spatial weight, which can be expressed by Equation (11)

$$y_i = \beta_0(u_i, v_i) + \sum_{k=1}^p \beta_k(u_i, v_i)x_{ik} + \epsilon_i \quad (11)$$

where y_i denotes the value of MST for grid i , (u_i, v_i) stands for the spatial location (latitude, longitude) of grid i ; p is the number of potential affecting factors of MST; $\beta_k(u_i, v_i)$ is the k th local regression parameter (coefficient) of grid i , varying with the location of grid i ; $\beta_0(u_i, v_i)$ is the intercept at a location (u_i, v_i) ; x_{ik} is the value of the k th explanatory variable of surface

temperature at grid i ; ϵ_i is the error term. Therefore, each grid across the entire surface of Mars in our research has a set of specific parameters to evaluate the relationships between MST and its potential affecting factors.

According to Tobler's first law of geography, everything is related to everything else, but near things are more related than distant things (Tobler 1970). Therefore, variables of the neighboring spatial units should contribute more than distant spatial units when calculating regression parameters (Wang et al. 2014). Bandwidths or neighbors are often used to determine the influence of spatial units at different geographical locations on the estimates of the local regression parameters. In this study, the optimal bandwidths for the GWR were determined by minimization of the corrected Akaike Information Criterion (AICc).

3. Results

3.1. Spatial-temporal Cluster Analysis of the MST

3.1.1. Global Spatial Autocorrelation of the MST

In order to test whether spatial aggregation for the MST exists, the global Moran's I was introduced to evaluate the degree of spatial autocorrelation for each monthly MST during the study period. Figure 2 demonstrates the variation of the Global Moran's I for monthly average surface temperature on the global area of Mars during the period of Martian years 30–32.

As plotted in Figure 2, the global Moran's I of the MST was nearly stable over time with a slight variation. The values of global Moran's I of all Martian months during the study period were significant ($p < 0.001$) for positive with a mean value of 0.99, which indicates a positive spatial autocorrelation for MST. The significance of Moran's I was validated by p -values which were < 0.001 for all months, indicating that the spatial distribution did not occur randomly for surface temperature in

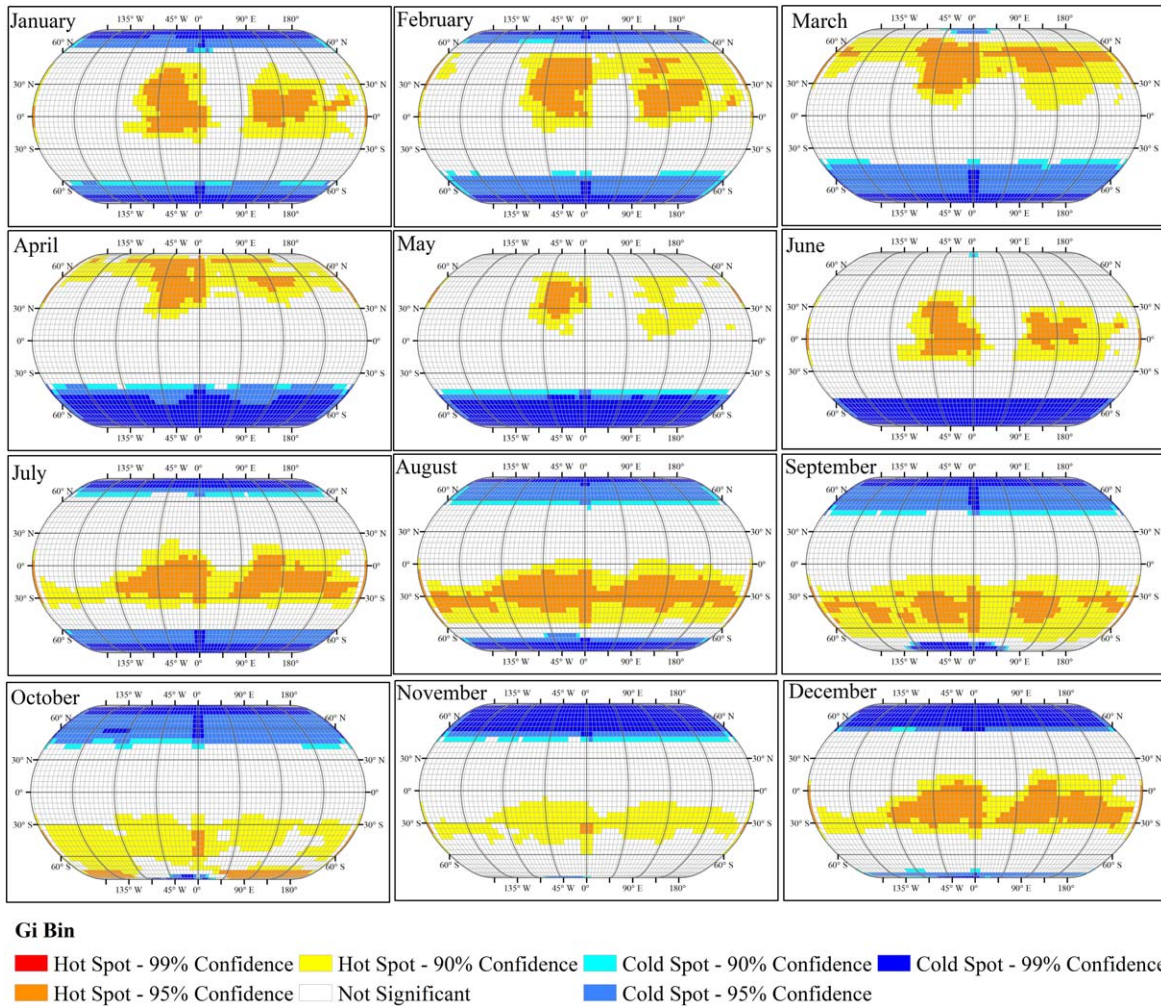


Figure 3. The hot spots and cold spots map for monthly surface temperature across global Mars in Martian year 30. The hot spots and cold spots were subdivided into several grades according to Gi Bin. The hot spots and cold spots maps of monthly MST in Martian years 31 and 32 are provided in the supplementary materials (Figures S1 and S2 respectively).

each Martian month. The z -score confirmed that the values were greater than 52.84 for all the 36 Martian months (see in Table S1 in the supplementary file), so there was nearly zero probability that the global surface temperature clustering pattern was a result of a stochastic process. The statistically significant high positive global Moran's I showed that the surface temperature was not randomly distributed but exhibited a definite pattern of spatial aggregation globally across Mars.

The Moran's I measures the degree of spatial autocorrelation of the MST at the global scale. The distribution of surface temperature, however, exhibits a heterogenous spatial pattern as the surface temperature has a certain degree of spatial similarity or difference in various locations, which leads to variation in spatial autocorrelation. Therefore, it is necessary to investigate the local patterns of surface temperature.

3.1.2. Local Cluster Analysis of MST

The GetisOrd G_i^* analysis was conducted to evaluate the local spatial clusters of monthly average surface temperature from Martian years 30–32 across Mars. The local clusters driven from the GetisOrd G_i^* model can be divided into hot spots (High–High clusters) and cold spots (Low–Low clusters). The results of the GetisOrd G_i^* analysis indicate the surface temperature agglomeration on Mars. The spatial patterns of hot spots and cold spots are illustrated in Figure 3. The spatial units in red represent significant hot spots, indicating that grid cells with high surface temperature are surrounded by other cells with similarly high surface temperatures. The cells in blue are significant cold spots, implying that the cells with low surface temperature are surrounded by other cells with similarly low surface temperatures.

Table 3

Multicollinearity Test in Northern Hemisphere Spring (Ls 0°–90°), Summer (Ls 90°–180°), Autumn (Ls 180°–270°), Winter (Ls 270°–360°), and Martian year 30–32 Groups

Variables	Unit	VIF				
		Spring	Summer	Autumn	Winter	Martian years 30–32
Ps	Pa	5.5	4.78	1.25	1.15	2.27
CO ₂	kg m ⁻²	1.33	...	1.37	1.31	1.37
Dust	NU	5.55	5.42	2.51	2.19	3.9
Slope	Degree (°)	1.56	1.54	1.64	1.63	1.62
Albedo		1.12	1.1	1.12	1.11	1.12
TI	tiu	1.29	1.4	1.2	1.29	1.19
Latitude	Degree (°)	2.62	2.61	3.29	2.47	4.24

As presented in Figure 3, the distribution of the spatial clusters of MST demonstrates spatio-temporal variation. The spatial pattern of MST clusters changed slightly from year to year, but varied significantly by month. The movement of the cold and hot spots in the north–south direction is related to the periodic revolution of Mars around the Sun and the large eccentricity of the orbital revolution, which is similar to that of the Earth. The hot spots are found in the low and middle latitudes (latitude range of 60°N–60°S) except during April and October, while the cold spots are concentrated in high latitudes (latitude >60°N or >60°S). Moreover, the hot spots are more widely distributed in the southern hemisphere than in the north, as Mars is near perihelion during the southern hemisphere’s summer. Overall, the results are consistent with known Martian climatic patterns (Read et al. 2015). This demonstrates that the season and the geographical locations explain the spatio-temporal variation in spatial aggregation and heterogeneity of surface temperature on Mars.

The hot spots in the northern and southern hemisphere are asymmetrical. Hot spots were widely and continuously distributed in the zonal direction (parallel to latitude) in the southern hemisphere from July to December. The hot spots in the northern hemisphere, especially in January, February, May and June, were relatively dispersed and divided into two clusters, as featured in Figure 3 and combining with the distribution of the topography, TI and albedo across the Martian surface in Figure S3 in the supplementary file. The hot spots are mainly distributed in low-lying basins with relatively high TI and low albedo (Figures S5 and S6). This implies that in addition to the huge orbital eccentricity of Mars, the MST might be affected by multiple factors. We discuss factors which may contribute to the spatial pattern of the MST using RF and GWR models in the next section.

3.2. Analysis of Factors Potentially Influencing MST

To explore the seasonal difference of the influence of factors potentially affecting MST, we divided the data during Martian years 30–32 into spring, summer, fall, winter and Martian year 30–32 groups. However, in the data set for each group, the

influencing factors were not independent and exhibited varying degrees of correlation. Thus, if all the potential influencing factors mentioned in Table 2 were chosen as independent variables for regression, a significant collinearity problem may occur in the regression models. To solve this issue, a multicollinearity test was introduced for each group before the analysis. We performed a stepwise regression model with all the variables and removed the independent variable if its variance inflation factor (VIF) value was greater than 7.5. We repeated the stepwise regression process mentioned until the VIF values of all independent variables were less than 7.5. Table 3 presents the multicollinearity test in the northern hemisphere spring, summer, fall, winter and Martian year 30–32 groups.

As seen in Table 3, the variables Ps, dust, slope, albedo, TI and latitude remained in the spring, fall, winter and Martian year 30–32 groups. The variables Ps, dust, slope, albedo, TI and latitude were selected for the summer group in an RF analysis to identify the globally dominant factors and further estimated the spatial difference among the factors influencing MST at the local scale using a GWR model.

3.2.1. The Variable Importance Ranking of Driven Factors for MST on a Global Perspective

The RF model was used to evaluate the effect of Ps, CO₂, dust, slope, albedo, TI and latitude for the MST from a global perspective, executed in the R language. The performance of the RF model was analyzed based on R^2 , root mean square error (RMSE) and mean absolute error (MAE).

As presented in Table 4, the RF model could account for 99.7%, 99.1%, 99.4%, 99.2% and 99.8% of the total MST in spring, summer, fall, winter and Martian years 30–32 respectively. The variable importance of the influencing factors is represented by the percentage of Increased Mean Square Error (%IncMSE).

Figure 4 graphs the variable importance evaluation of selected affecting factors based on RF model during spring, summer, fall, winter and Martian years 30–32.

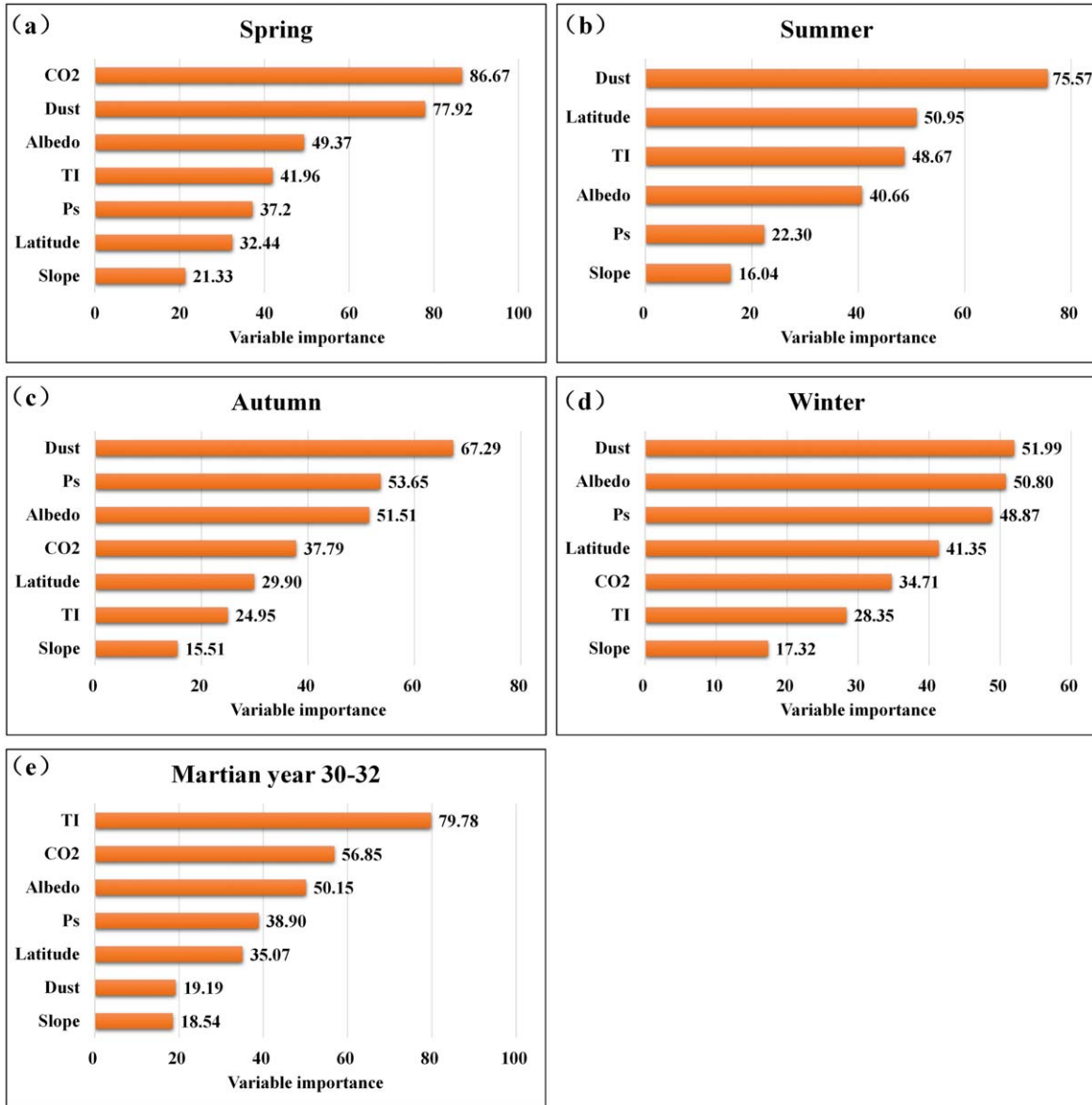


Figure 4. Variable importance of selected affecting factors based on RF during northern hemisphere spring (a), summer (b), fall (c), winter (d) and Martian years 30–32 (e).

Table 4
The Performance of RF

Group	R^2	RMSE	MAE
Spring	0.9971	1.4338	0.8258
Summer	0.9919	2.5133	1.2239
Autumn	0.9939	2.6274	1.3615
Winter	0.9916	2.9471	1.4031
Martian years 30–32	0.9985	0.8284	0.5603

The influence of the factors on MST displayed conspicuous seasonal differences (Figure 4). CO₂ was the most important variable (86.67) for explaining the variation of MST in spring, as displayed in Figure 4(a). Dust was the second most

important variable influencing surface temperature in spring. In contrast, dust was found to provide the greatest contribution in affecting surface temperature in summer (Figure 4(b)), fall (Figure 4(c)) and winter (Figure 4(d)). In addition, latitude, Ps and albedo played the second most important role in affecting surface temperature in summer, fall and winter respectively. The slope was the least important factor for surface temperature compared with other affecting factors during all seasons. For the period during Martian years 30–32, the three most relevant variables were TI, CO₂ and albedo (Figure 4(e)). The RF ranked the variable importance of driven factors for MST with a high model fit. It assumes that the MST and its driving factors are spatially consistent, thus it cannot identify the dominant

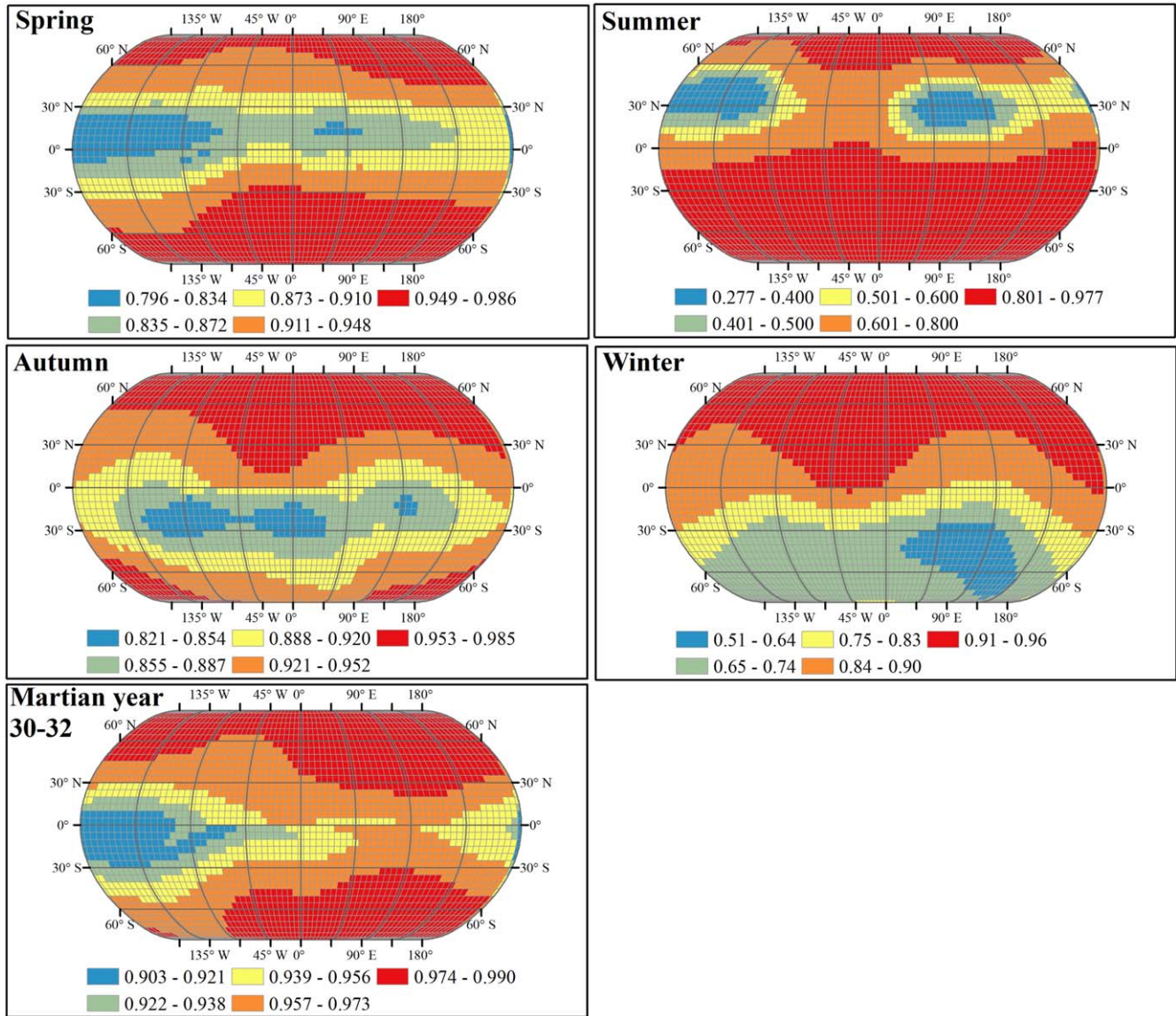


Figure 5. Spatial distribution of local R^2 based on the GWR model during northern hemisphere spring (Ls 0° – 90°), summer (Ls 90° – 180°), fall (Ls 180° – 270°), winter (Ls 270° – 360°) and Martian years 30–32.

factors at different locations. However, the MST and driving factors varied with location.

The regional difference in spatially aggregated pattern (Figure 3) of surface temperature implies that the distribution of surface temperature may be caused by some potential locally driven factors. Clearly, the global models are not adequate to explore the spatial variation of the correlation between variables, because they assume that all the variables and their relationships are stable over space. A local regression model could account for the local difference to detect the relations between MST and potential affecting factors. The GWR model can estimate the difference in the relationships between MST and the driving factors in various geographical regions.

3.2.2. Spatial Heterogeneity in the Relationships between MST and Driving Factors from a Local Perspective

We used the GWR model to estimate the regional difference in the relationships between MST and its potential driving factors. The performance of the GWR model was analyzed using R^2 , Adjusted R^2 and AICc, a corrected version of Akaike Information Criterion. As presented in Table 5, the GWR model could account for 97.3%, 97.9%, 97.4%, 95.0% and 98.4% of the total MST in spring, summer, fall, winter and Martian years 30–32 respectively.

Furthermore, the spatial heterogeneity of local fitting degree of GWR was evaluated by local R^2 . The spatial variations of local R^2 are displayed in Figure 5.

Table 5
Evaluating the Performance of the GWR Model

Groups	R^2	Adjusted R^2	AICc
Spring	0.974	0.9733	15 036.5
Summer	0.9799	0.9792	14 683.7
Autumn	0.9743	0.9736	16 058.4
Winter	0.9507	0.9497	17 480
Martian years 30–32	0.9846	0.9841	12 359.1

As affirmed in Figure 5, all the local R^2 values were greater than 0.796, 0.821 and 0.903 in spring, fall and Martian year 30–32 groups respectively, indicating that the GWR model performed well at each local location over the whole of Mars during these periods. Except for the low and middle latitudes of the northern hemisphere, the values of local R^2 were higher than 0.8 in the summer; only in a small part of the middle latitudes were the local R^2 values less than 0.5. For the winter group, the local R^2 values varied from 0.51 to 0.90, and local R^2 values in the northern hemisphere were all higher than 0.8; only a small part in the southeast of the southern hemisphere had local R^2 values of less than 0.65. The diagnostics affirm that the GWR model is adequate to detect the influence of the driving factors for MST at a local scale. We mapped the spatial heterogeneity of the relationships between potential driving factors (including TI, CO_2 , albedo, Ps, latitude, dust and slope) and MST during spring (Figure 6), summer (Figure 7), fall (Figure 8), winter (Figure 9) and Martian years 30–32 (Figure 10) based on the analysis of the GWR. The coefficients of each driving factor varied with season and location. The effect of each factor on surface temperature displays a unique spatial pattern across Mars in every season. The local coefficients of the GWR model imply that each influencing factor showed significant spatial difference in positive and negative correlation with MST across Mars. In general, the distribution of local coefficients for factors driving MST in each group was not randomly distributed but followed a certain spatial pattern, as manifested in spatial agglomeration and gradient directionality. A detailed analysis of each group is as follows:

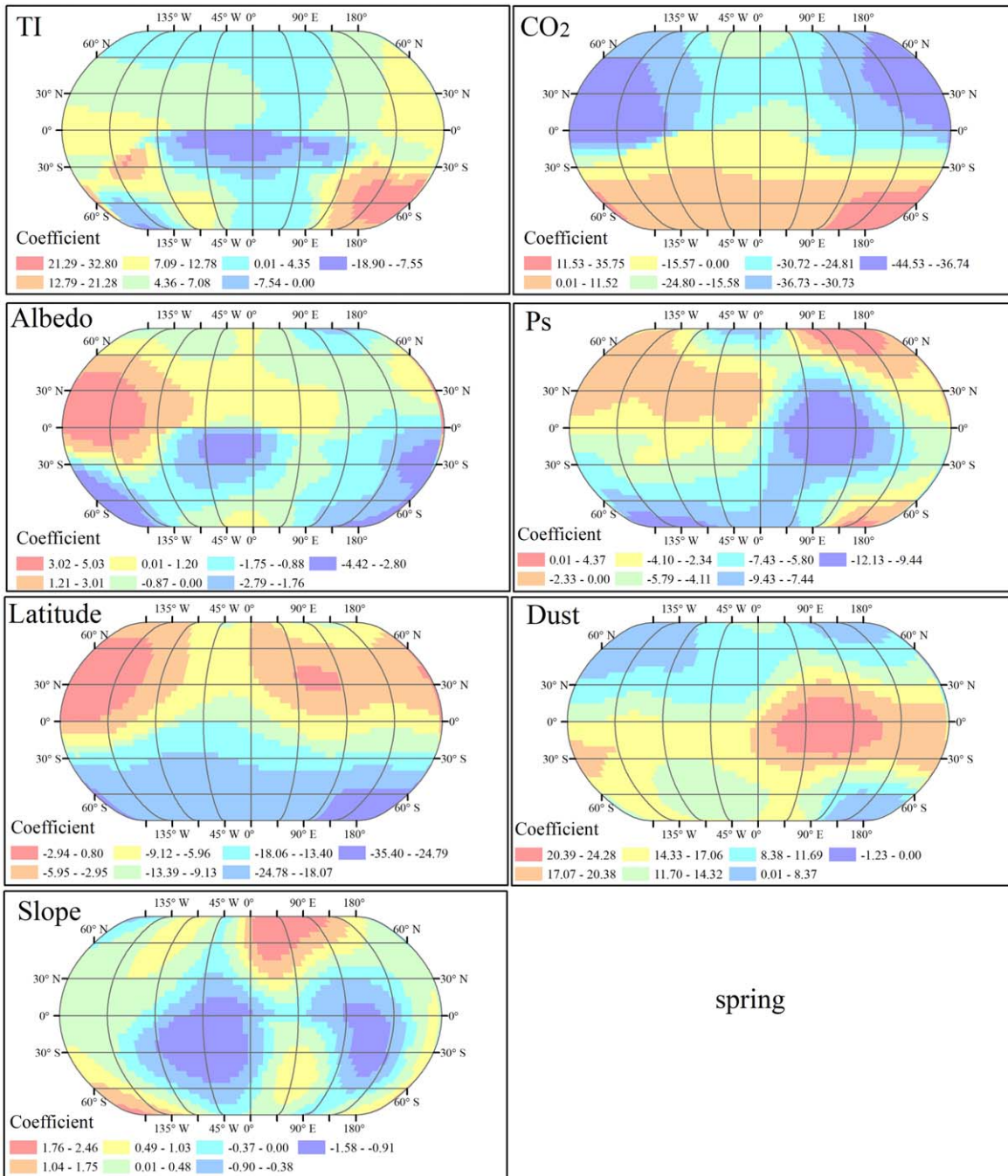
In northern spring as depicted in Figure 6, the distribution pattern of surface temperature was highly correlated with TI, CO_2 , Ps, latitude and dust. Local coefficient of TI values ranged widely from 18.9 to 32.8. The TI has a positive correlation with the surface temperature in 90% of cells of Mars, especially in Promethei Terra (Figure S4) in the high and middle latitudes of the southern hemisphere; while a negative correlation in Margaritifer Terra near the equator. The CO_2 had a significantly negative impact on MST in 71% of the area of the Martian surface, such as the northern hemisphere, and low latitudes in the southern hemisphere; while a positive

coefficient in the high and middle latitudes of the southern hemisphere. Ps exhibited a negative relation with the surface temperature across Mars, and especially in Syrtis Major Planum, Isidis Planitia, Tyrrhena Terra and Terra Sabaea. Latitude exhibited a negative relationship with MST, and the negative coefficient was greater in the south. Dust was positively correlated with the MST in most areas of Mars and the positive correlation was greater within low latitude regions, especially in Syrtis Major Planum, Tyrrhena Terra and Terra Sabaea.

In northern summer (Figure 7), the pattern of surface temperature was highly affected by TI, Ps, latitude and dust, and the spatial pattern of each factor's coefficient was different from that in the spring. TI had a negative relationship with MST in most areas (87% of the Martian surface), especially in Copernicus Crater, Stoney Crater and Promethei Rupes; while there was a positive correlation in Deadalia Planum, Syria Planum and Tyrrhena Terra. Dust exhibited a positive relation in the southern hemisphere, especially in Terra Sabaea and Terra Cimmeria; while a negative relevance near the north pole. Latitude manifests a strong negative correlation with the surface temperature in the southern hemisphere. The correlation between Ps and surface temperature was positive in the north and negative in the south, especially in the polar regions.

In northern fall (Figure 8), the distribution pattern of surface temperature was highly influenced by TI, CO_2 , albedo, Ps, latitude and dust. TI has a positive correlation with the surface temperature in the southern hemisphere, and shows a great positive coefficient in the regions near the south pole. The CO_2 and surface temperature displayed a strong negative correlation in low latitudes, and a positive correlation at the north pole. Albedo was negatively correlated with surface temperature, and exhibited a large negative impact on surface temperature in Amazonis Planitia, Olympus Mons and Tharsis Montes. Latitude was negatively correlated with the surface temperature, and was greatest at the poles, especially the Arctic. The Ps had a strong negative correlation with surface temperature in the tropics near the equator. Dust had a great relevance with the surface temperature in the southern hemisphere, showing a strong negative correlation in the west of Planum Australe near the Antarctic, and a strong positive correlation near the equator.

In northern winter (Figure 9), the distribution pattern of surface temperature was highly influenced by TI, CO_2 , albedo, Ps, latitude and dust. The distribution of latitude, dust, albedo and Ps coefficients was similar to that in fall. CO_2 had a great negative correlation with the surface temperature in Promethei Terra, Terra Cimmeria and Tyrrhena Terra. TI was positively related with the MST in Aonia Terra and Promethei Terra. Slope was positively correlated with surface temperature in Promethei Terra, Terra Cimmeria and Hellas Planitia.



spring

Figure 6. The spatial variation of the local coefficient for the affecting variables (TI, R^2 , albedo, Ps, latitude, dust and slope) using the GWR model during northern hemisphere spring (Ls 0°–90°).

In Martian years 30–32 (Figure 10), TI was positively correlated with surface temperature, and the coefficient in the southern hemisphere was larger than that for the northern hemisphere. The influence of CO₂ ice on surface temperature increased from south to north, with a gradient distribution trend. The regression coefficient was between -25.66 – 2.67 .

The albedo and pressure had a great negative relationship with the MST in the southern hemisphere. Surface temperature in the southern hemisphere was more influenced by latitude than in the northern hemisphere. Dust had a high positive correlation with surface temperature in Hellas Planitia, Melea Planum and Terra Sirenum.

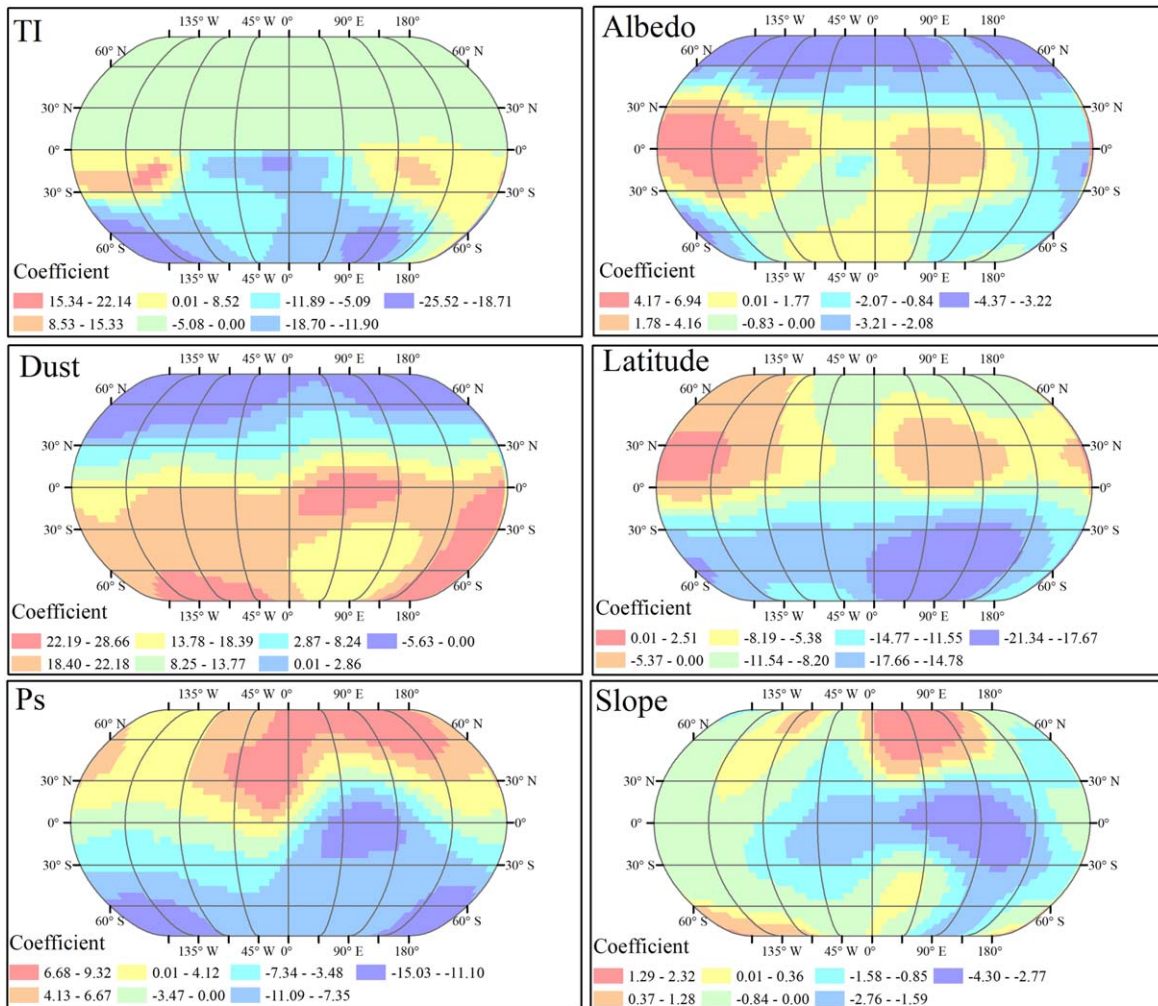


Figure 7. The spatial variation of the local coefficient for the affecting variables (TI, albedo, dust, latitude, Ps and slope) using the GWR model during northern hemisphere summer (Ls 90°–180°).

4. Discussion

Taking 2592 grid cells across the Martian surface as the research object, this paper detects the spatial clusters of MST by spatial autocorrelation analysis and analyzes the influencing factors of MST across global Mars from Martian years 30 to 32 by using the RF and GWR model. The results of spatial autocorrelation analysis show that the MST is spatially clustered, and local clusters have huge latitude differences. The cold spots and hot spots move in the north–south direction with seasonal changes. The large seasonal variations in the MST hotspots are partly due to variations in solar heating associated with orbital eccentricity (Kahn et al. 1992; Richardson & Wilson 2002).

In addition to the uneven distribution of MST hot spots at different latitudes, the hot spots of MST are also unevenly distributed in the same latitude. The discontinuous distribution

of hot spots in the northern hemisphere in the zonal direction might be related to hemispheric topographic asymmetry or the TI and albedo. The huge topographical difference in mid-latitudes, and asymmetric hemispheric topography could play a major role in altering the strengths of the meridional and small scaled circulation in summer (Zalucha et al. 2010). Moreover, the surface covered with high albedo materials will radiate heat more efficiently and absorb less sunlight than darker materials, therefore staying cooler throughout the summer (Haberle et al. 2017). A surface with low TI can heat up and cool down quickly, thus retaining a cool temperature.

On top of topographic asymmetry, TI and albedo, the heterogeneous distribution of surface temperature might be caused by some potential local driven factors. We utilized the GWR to estimate the regional difference in the relationships between MST and the driving factors. The results of GWR

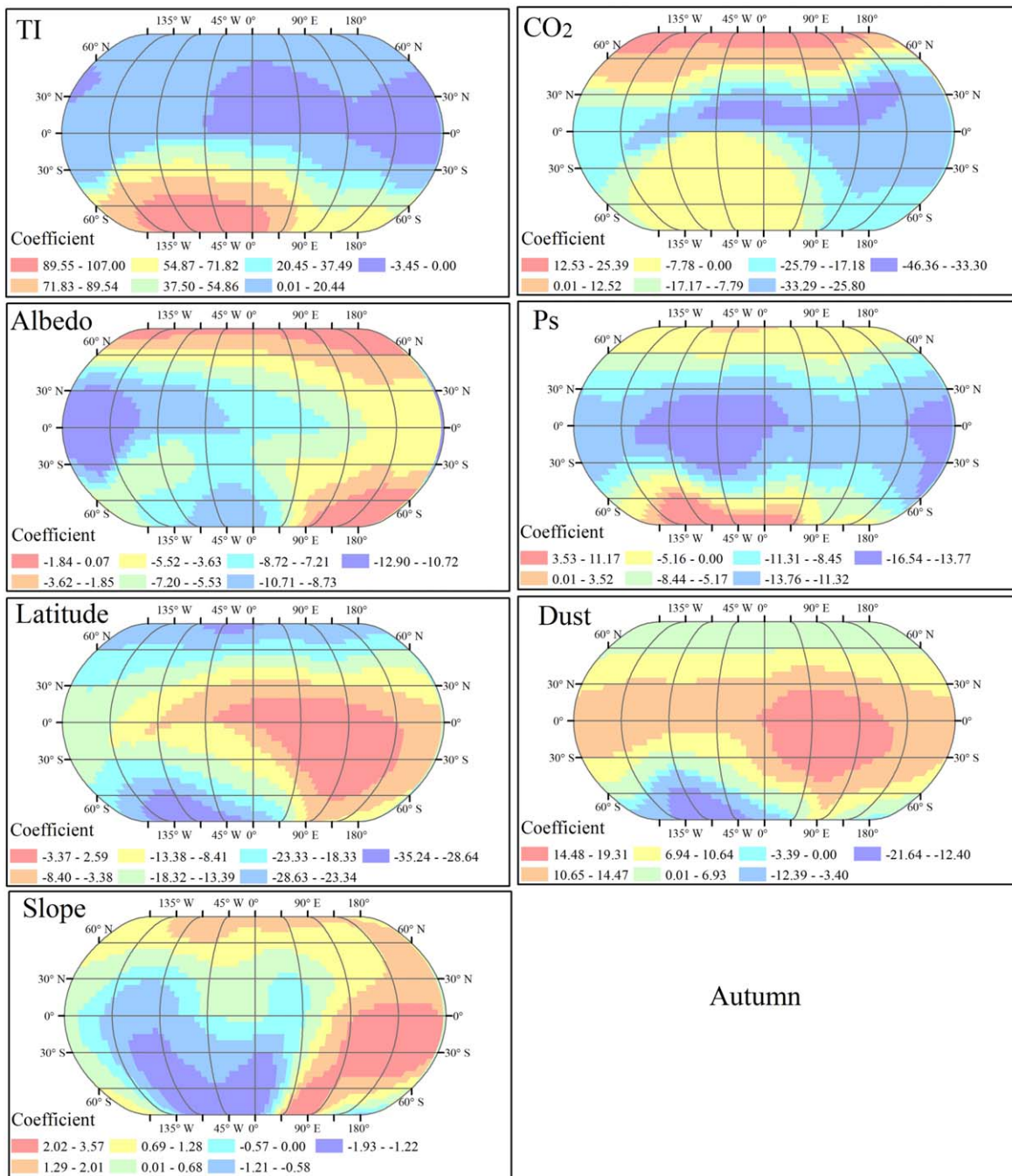
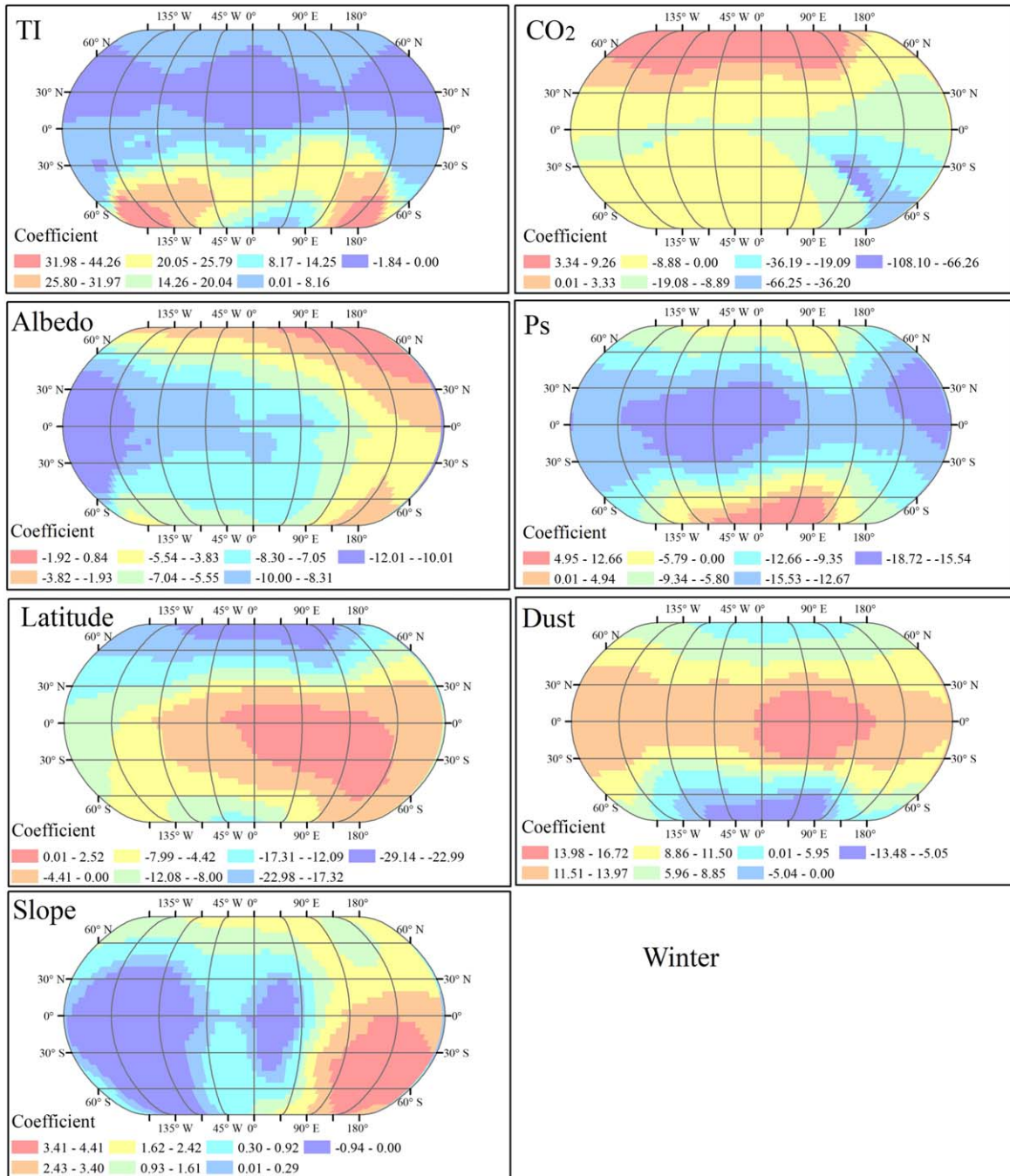


Figure 8. The spatial variation of the local coefficient for the affecting variables (TI, CO₂, albedo, Ps, latitude, dust and slope) using the GWR model during northern hemisphere fall (Ls 180°–270°).

confirm that the influence of each factor on MST has seasonal and spatial differences.

The dependence of surface temperature on TI was greater in the southern hemisphere through all seasons as displayed in Figures 6–9, compared with the northern hemisphere. The TI is relatively low in the Martian southern hemisphere, especially the

south pole and the altitude is higher compared with the northern hemisphere. Mesoscale winds are prone to occur on steep slopes with low TI (Spiga et al. 2011), and affect the balance of surface energy budget. Thus, the mesoscale Martian atmospheric wind has a particularly strong influence on the surface temperature in the southern hemisphere with steeper slopes and lower TI.

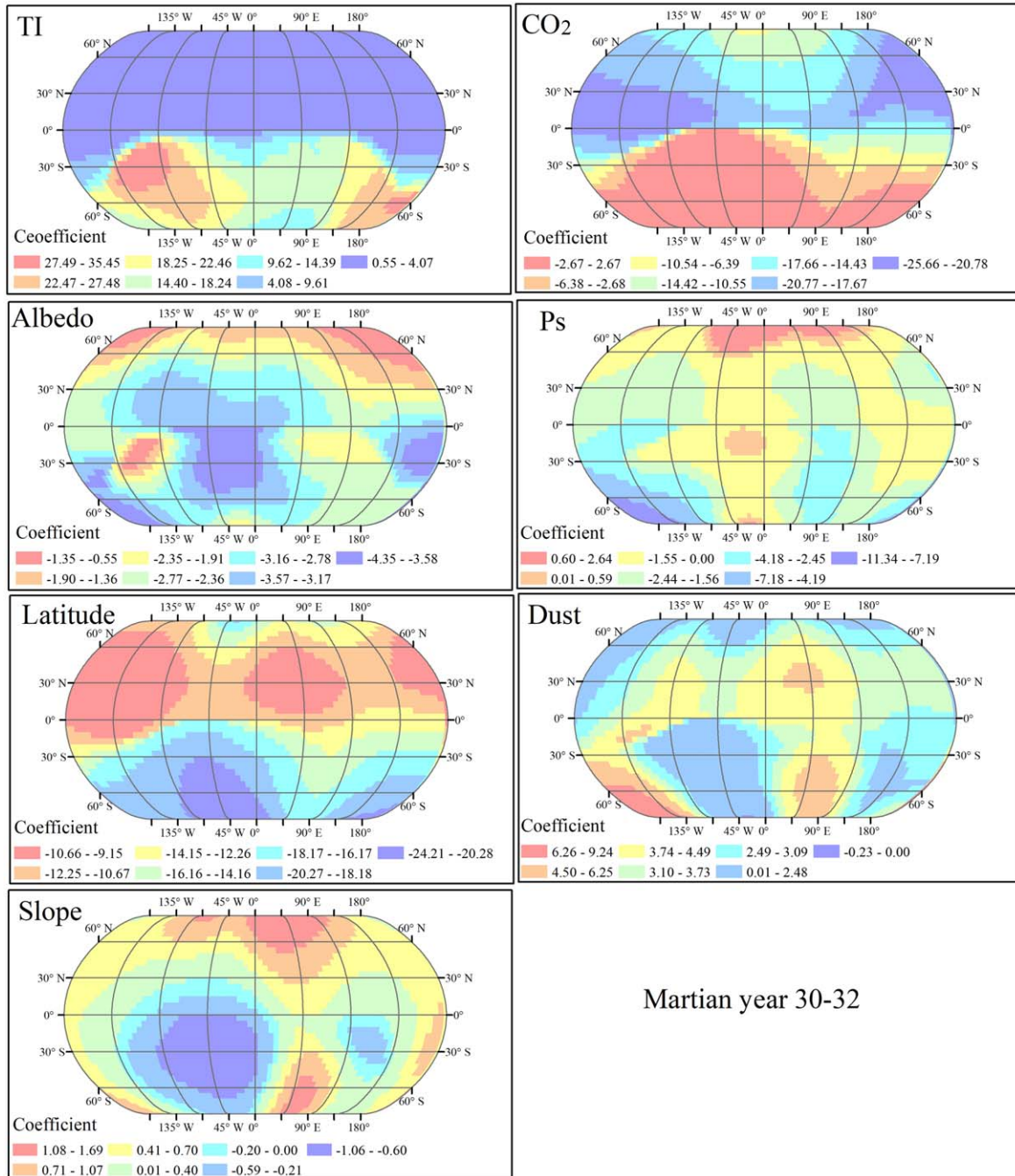


Winter

Figure 9. The spatial variation of the local coefficient for the affecting variables (TI, CO₂, albedo, Ps, latitude, dust and slope) using the GWR model during northern hemisphere winter (Ls 270°–360°).

The regions with high CO₂ ice coefficient value moved from north to south from southern spring to winter. The area highly affected by CO₂ ice was in the northern hemisphere in spring, in the area near the equator in fall, and in the southern hemisphere in winter as depicted in Figures 6 and 7. This could be explained by the seasonal circulation controlled by the

condensation and sublimation of CO₂ in high latitudes (Haberle et al. 2017), which has a crucial influence on the MST. The CO₂ cycle mainly depends on the intensity of solar radiation, so the polar CO₂ ice abundance manifests significant seasonal differences, and its impact on the climate also varies seasonally. The impact of CO₂ on surface temperature was



Martian year 30-32

Figure 10. The spatial variation of the local coefficient for the affecting variables (TI, CO₂, albedo, Ps, latitude, dust and slope) using the GWR model during Martian years 30–32.

significantly different in the eastern and western hemispheres of the south polar region, because the surface topography can alter the CO₂ cycle by generating atmospheric gravity waves, and the gravity waves can change the type and amount of CO₂ ice deposits (Haberle et al. 2017). This occurs in the southern hemisphere, due to the huge topographical differences in the

southern hemisphere, such as the Tharsis Plateau in the south and the Hellas and Argyre Basins, which cause differences in the relationship between surface temperature and CO₂ in the eastern and western hemispheres of Antarctica (Colaprete et al. 2005). In addition, dust can also alter the sublimation rate of carbon dioxide ice (Gary-Bicas et al. 2020).

The albedo had a great influence on the surface temperature near the equator in northern fall and winter, especially in Amazonis Plantia with a high albedo, as we can infer from Figures 8 and 9. Surface albedo is primarily responsible for the amount of solar energy reflected or absorbed by the Martian surface (Singh 2020). In the southern spring and summer, Mars is close to the Sun, and the surface could receive a large amount of solar radiation. Therefore, the relationship between albedo and solar radiation is stronger in southern spring and summer compared with northern spring and summer, which makes regions with high albedo become colder in these seasons, and this is especially obvious in low latitudes.

The relationship between latitude on surface temperature was negative as shown in Figures 6–9, and the most correlated areas were the southern hemisphere in spring and summer, near the north pole in fall, and in the northern hemisphere in winter. This is mainly related to the eccentric orbit of Mars. However, the surface temperature of the same latitude zone was not the same, and the response degree with latitude was also different. This is due to the heterogeneity of multiple surface elements, such as the difference in local topography, TI and albedo in the same latitude.

The spatial pattern of the influence intensity of Ps and dust on surface temperature was similar in each season as depicted in Figures 6–9. Ps had a great negative correlation with the surface temperature in the tropical and subtropical regions during the northern fall and winter, while the dust had a positive influence on the surface temperature. The large impact of Ps and dust on the surface temperature mainly occurred in the tropical and subtropical regions in northern fall and winter, which was related to the strong Hadley circulation, thermal tides and topographically forced flow in the low latitudes regions (Leovy et al. 1973). Hadley circulation is a heat-driven circulation which was caused by the air rising at warm latitudes and descending at cold latitudes (Guendelman & Kaspi 2018). The Hadley circulation is controlled by solar heating, so circulation varied with seasons. The Hadley circulation has a strong control on the transportation of dust. Dust particles in the atmosphere absorb and radiate solar radiation, so the surface mean temperature is strongly controlled by dust suspended in the atmosphere (Leovy 2001). In northern summer, Ps and dust had a stronger correlation with surface temperature in the southern hemisphere compared with the northern hemisphere. This could be explained by the hemispheric difference in atmosphere circulation. The hemispherical asymmetry of tropical and subtropical circulation intensity is related to the Martian eccentricity and the huge hemispheric difference in topography (Richardson & Wilson 2002; Zalucha et al. 2010; Wilson 2012). The circulation is stronger in southern winter (northern summer) in the southern hemisphere. The heated dust in the air further expands the scope of the Hadley circulation and thermal tides. In northern spring, the Ps and dust had a large negative impact on surface temperature in

Syrtis Major Planum, Terra Sabaea and Tyrrhena Terra in the tropics.

The terrain slope was used to investigate the correlation between the MST and topographic conditions. Variations in the slope had less effect on the surface temperature compared with the latitude location and the near surface properties such as TI, albedo, Ps, dust. The topography affects the surface temperature mainly by changing the atmospheric heat transportation. On Mars, the topography has less effect on the surface temperature than on Earth, because the atmosphere density on Mars is much less than that on Earth, and the atmospheric heat convection and transport are relatively weaker than on Earth (Read et al. 2015).

However, in the analysis of influencing factors of MST, due to the limitation of data acquisition and the complex MST mechanisms which are not yet understood, the influencing factors of the MST involved in this study are not comprehensive. We only focused on some potential main factors that may affect surface temperature. In addition, our paper only studied the spatial and seasonal variation in the relationships between MST and its potential influencing factors, but whether these relationships are causal needs to be further investigated.

5. Conclusion

This study investigated the spatial autocorrelation of MST during Martian years 30–32 across global Mars, and further quantitatively estimated the seasonal effect of the potential near-surface meteorological and environmental factors on the surface temperature for each local region.

The results indicate that the MST presents significant spatial aggregation, and hot spot and cold spot distribution patterns display hemispheric asymmetry and seasonal variations. The hemispheric asymmetry of hot spots is caused by the hemispheric asymmetry in topography and surface TI and albedo, which can primarily account for the differing hemispheric strengths of the meridional or small scale circulation in summer. The discontinuous distribution of hot spots in the northern hemisphere was caused by the huge topographical difference in mid-latitudes, and the hot spots were distributed in low-lying basins with relatively high TI and low albedo.

The spatio-temporal pattern of the MST depends on the spatial and seasonal variation of meteorological and environmental factors. The difference in dominant factors in different locations identified by the GWR model was related to the differences in local geography and climate for local regions across Mars. The surface temperature was greatly affected by the latitude locations but the influence in the same latitude zone was not stable. This was caused by heterogeneity of multiple near surface environmental elements, such as the difference in local topography, TI and albedo in the same latitude. The strong seasonal Hadley circulation and topographically forced flow were primarily responsible for the variation of surface

temperature in low-latitudes. Due to the seasonal change and asymmetry of the Hadley circulation at low latitudes, the Ps and dust had a strong correlation with the surface temperature in the tropical and subtropical regions in northern fall and winter, while in the southern hemisphere, they show a stronger correlation compared with the northern hemisphere in northern summer. The polar regions were greatly affected by the seasonal circulation controlled by the condensation and sublimation of CO₂. The surface temperature in the southern hemisphere was more sensitive to environmental factors compared with the northern hemisphere because of the larger amplitude topography and lower TI in the southern hemisphere.

This study offers a new quantitative insight in understanding the spatio-temporal variation in spatial autocorrelation and heterogeneity of the MST. The findings remind us to focus on the spatial autocorrelation, as well as its variations with geographical locations and seasons when simulating Martian climate models. In addition, we emphasize that regional and seasonal variation of the driving factors are critical in understanding the MST distribution patterns and ignoring these spatio-temporal aspects when simulating Martian climate may cause inaccuracy of models. Our present study was based on statistical methods combining GIS. We hope that the findings will encourage more process-based explorations into the spatial autocorrelation pattern and spatio-temporal potential driving factors of other phenomena on Mars.

Acknowledgments

We are grateful to NASA for providing models to make this research possible. J.Y. is supported by the pre-research Project on Civil Aerospace Technologies (No. D020103), F.L. and J.G. are supported by the National Natural Science Foundation of China (Grant No. 42030110).

ORCID iDs

Jian-Guo Yan  <https://orcid.org/0000-0003-2612-4776>

References

- Breiman, L. 2001, *Mach. Learn.*, 45, 5
- Brunsdon, C., Fotheringham, A. S., & Charlton, M. E. 1996, *Geographical Analysis*, 28, 281
- Cai, H., Lam, N. S., Qiang, Y., et al. 2018, *IJDRR*, 31, 844
- Christensen, P. R., Bandfield, J. L., Hamilton, V. E., et al. 2001, *JGRE*, 106, 23823
- Colaprete, A., Barnes, J. R., Haberle, R. M., et al. 2005, *Natur*, 435, 184
- Fenton, L. K., Geissler, P. E., & Haberle, R. M. 2007, *Natur*, 446, 646
- Ferguson, R. L., Hare, T. M., & Laura, J. 2018, HRSC and MOLA Blended Digital Elevation Model at 200m v2. Astrogeology PDS Annex, U.S. Geological Survey, http://bit.ly/HRSC_MOLA_Blend_v0
- Fotheringham, A. S., Brunsdon, C., & Charlton, M. 2003, *Geographically Weighted Regression: The Analysis of Spatially Varying Relationships* (New York: Wiley)
- Gary-Bicas, C., Hayne, P., Horvath, T., et al. 2020, *JGRE*, 125, e2019JE006150
- Getis, A. 2010, *Handbook of Applied Spatial Analysis* (Berlin: Springer), 255
- Grömping, U. 2009, *AmStat*, 63, 308
- Guendelman, I., & Kaspi, Y. 2018, *GeoRL*, 45, 13
- Gurwell, M. A., Bergin, E. A., Melnick, G. J., & Tolls, V. 2005, *Icar*, 175, 23
- Haberle, R. M., Clancy, R. T., Forget, F., Smith, M. D., & Zurek, R. W. 2017, *The Atmosphere and Climate of Mars* (Cambridge: Cambridge Univ. Press)
- Hamilton, V. E., Vasavada, A. R., Sebastián, E., et al. 2014, *JGRE*, 119, 745
- Holmes, J. A., Lewis, S. R., & Patel, M. R. 2020, *P&SS*, 188, 104962
- Hunt, G. E. 1980, *GeoRL*, 7, 481
- Ishwaran, H. 2007, *EJSta*, 1, 519
- Jakosky, B. M., Mellon, M. T., Kieffer, H. H., et al. 2000, *JGRE*, 105, 9643
- Kahn, R., Martin, T., Zurek, R., & Lee, S. 1992, in *Mars*, ed. H. H. Kieffer (Tucson, AZ: Univ. Arizona Press)
- Kass, D., Kleinböhl, A., McCleese, D., Schofield, J., & Smith, M. 2016, *GeoRL*, 43, 6111
- Kass, D., Schofield, J., Kleinböhl, A., et al. 2020, *GeoRL*, 47, e2019GL083931
- Kieffer, H. H., Chase, S. C., Miner, E. D., et al. 1976, *Sci*, 193, 780
- Kieffer, H. H., Martin, T., Peterfreund, A. R., et al. 1977, *JGR*, 82, 4249
- Kieffer, H. H., Neugebauer, G., Munch, G., Chase, S., Jr., & Miner, E. 1972, *Icar*, 16, 47
- Leovy, C. 2001, *Natur*, 412, 245
- Leovy, C., Zurek, R., & Pollack, J. 1973, *JAtS*, 30, 749
- Liaw, A., & Wiener, M. 2002, *R News*, 2, 18
- Martínez, G., Newman, C., De Vicente-Retortillo, A., et al. 2017, *SSRv*, 212, 295
- Mellon, M. T., Jakosky, B. M., Kieffer, H. H., & Christensen, P. R. 2000, *Icar*, 148, 437
- Miller, N., de la Torre Juárez, M., & Tamppari, L. 2018, *GeoRL*, 45, 11
- Millot, C., Quantin-Nataf, C., Leyrat, C., & Enjolras, M. 2021, *Icar*, 355, 114136
- Moran, P. A. 1950, *Biometrika*, 37, 17
- Ord, J. K., & Getis, A. 1995, *Geographical Analysis*, 27, 286
- Petrosyan, A., Galperin, B., Larsen, S. E., et al. 2011, *RvGeo*, 3, 49
- Pierrehumbert, R. T. 2010, *Principles of Planetary Climate* (Cambridge: Cambridge Univ. Press)
- Piqueux, S., & Christensen, P. R. 2011, *JGRE*, E7, 116
- Putzig, N. E., & Mellon, M. T. 2007, *Icar*, 191, 68
- Read, P., Lewis, S., & Mulholland, D. 2015, *RPPH*, 78, 125901
- Richardson, M. I., & Wilson, R. J. 2002, *Natur*, 416, 298
- Savijärvi, H. 1999, *QJRM*, 125, 483
- Siegler, M. A., Smrekar, S. E., Grott, M., et al. 2017, *SSRv*, 211, 259
- Singh, D. 2020, *E&PP*, 4, 206
- Smith, P. F., Ganesh, S., & Liu, P. 2013, *JNeurosciMethods*, 220, 85
- Spanovich, N., Smith, M., Smith, P., et al. 2006, *Icar*, 180, 314
- Spiga, A., & Forget, F. 2009, *JGRE*, E2, 114
- Spiga, A., Forget, F., Madeleine, J.-B., et al. 2011, *Icar*, 212, 504
- Strobl, C., Boulesteix, A.-L., Kneib, T., Augustin, T., & Zeileis, A. 2008, *BMC Bioinf.*, 9, 307
- Strobl, C., Boulesteix, A.-L., Zeileis, A., & Hothorn, T. 2007, *BMC Bioinf.*, 8, 1
- Tobler, W. R. 1970, *EconGeo*, 46, 234
- Tosi, F., Capaccioni, F., Capria, M. T., et al. 2019, *NatAs*, 3, 649
- Vasavada, A. R., Piqueux, S., Lewis, K. W., Lemmon, M. T., & Smith, M. D. 2017, *Icar*, 284, 372
- Wang, S., Fang, C., Ma, H., Wang, Y., & Qin, J. 2014, *JGeogSci*, 24, 612
- Wilson, R. 2012, *CCTP*, 1675, 8069
- Zalucha, A. M., Plumb, R. A., & Wilson, R. J. 2010, *JAtS*, 67, 673
- Zurek, R. W., Barnes, J. R., Haberle, R. M., et al. 1992, *Mars*, 835